Published in final edited form as:
J Control Release. 2020 July 10; 323: 269–281. doi:10.1016/j.jconrel.2020.04.030.

Nanobody-targeted photodynamic therapy induces significant tumor regression of trastuzumab-resistant HER2-positive breast cancer, after a single treatment session

Marion M. Deken[#a], **Marta M. Kijanka**[#b], **Irati Beltrán Hernández**[c], **Maxime D. Slooter**[d,2], **Henriette S. de Bruijn**[e], **Paul J. van Diest**[f], **Paul M.P. van Bergen en Henegouwen**[b], **Clemens W.G.M. Lowik**[g], **Dominic J. Robinson**[a,e], **Alexander L. Vahrmeijer**[a], **Sabrina Oliveira**[b,c,*]

[a]Dept. of Surgery, Leiden University Medical Center, Leiden, the Netherlands [b]Division of Cell Biology, Neurobiology and Biophysics, Dept. of Biology, Faculty of Science, Utrecht University, Utrecht, the Netherlands [c]Pharmaceutics, Dept. of Pharmaceutical Sciences, Faculty of Science, Utrecht University, Utrecht, the Netherlands [d]Dept. of Radiology, Division of Molecular Imaging, Leiden University Medical Center, Leiden, the Netherlands [e]Dept. of Otorhinolaryngology & Head and Neck Surgery, Center for Optical Diagnostics and Therapy, Erasmus Medical Center, Rotterdam, the Netherlands [f]Dept. of Pathology, University Medical Center Utrecht, Utrecht, the Netherlands [g]Dept. of Radiology, Optical Molecular Imaging, Erasmus University Medical Center, Rotterdam, the Netherlands

[#] These authors contributed equally to this work.

Abstract

Rationale—A substantial number of breast cancer patients with an overexpression of the human epidermal growth factor receptor 2 (HER2) have residual disease after neoadjuvant therapy or become resistant to trastuzumab. Photodynamic therapy (PDT) using nanobodies targeted to HER2 is a promising treatment option for these patients. Here we investigate the *in vitro* and *in vivo* antitumor efficacy of HER2-targeted nanobody-photosensitizer (PS) conjugate PDT.

Methods—Nanobodies targeting HER2 were obtained from phage display selections. Monovalent nanobodies were engineered into a biparatopic construct. The specificity of selected nanobodies was tested in immunofluorescence assays and their affinity was evaluated in binding studies, both performed in a panel of breast cancer cells varying in HER2 expression levels. The selected HER2-targeted nanobodies 1D5 and 1D5-18A12 were conjugated to the photosensitizer IRDye700DX and tested in *in vitro* PDT assays. Mice bearing orthotopic HCC1954 trastuzumab-resistant tumors with high HER2 expression or MCF-7 tumors with low HER2 expression were intravenously injected with nanobody-PS conjugates. Quantitative fluorescence spectroscopy was

[*]Corresponding author at: Dept. Biology & Pharmaceutical Sciences, Faculty of Science, Utrecht University, Padualaan 8, 3584 CH Utrecht, the Netherlands. s.oliveira@uu.nl (S. Oliveira).
[2]Currently Dept. of Surgery, Amsterdam UMC, University of Amsterdam, Amsterdam, The Netherlands.

Declaration of Competing Interest
The authors have declared that no competing interest exists.

Europe PMC Funders Author Manuscripts

performed for the determination of the local pharmacokinetics of the fluorescence conjugates. After nanobody-PS administration, tumors were illuminated to a fluence of 100 $J \cdot cm^{-2}$, with a fluence rate of 50 $mW \cdot cm^{-2}$, and thereafter tumor growth was measured with a follow-up until 30 days.

Results—The selected nanobodies remained functional after conjugation to the PS, binding specifically and with high affinity to HER2-positive cells. Both nanobody-PS conjugates potently and selectively induced cell death of HER2 overexpressing cells, either sensitive or resistant to trastuzumab, with low nanomolar LD_{50} values. *In vivo*, quantitative fluorescence spectroscopy showed specific accumulation of nanobody-PS conjugates in HCC1954 tumors and indicated 2 h post injection as the most suitable time point to apply light. Nanobody-targeted PDT with 1D5-PS and 1D5-18A12-PS induced significant tumor regression of trastuzumab-resistant high HER2 expressing tumors, whereas in low HER2 expressing tumors only a slight growth delay was observed.

Conclusion—Nanobody-PS conjugates accumulated selectively *in vivo* and their fluorescence could be detected through optical imaging. Upon illumination, they selectively induced significant tumor regression of HER2 overexpressing tumors with a single treatment session. Nanobody-targeted PDT is therefore suggested as a new additional treatment for HER2-positive breast cancer, particularly of interest for trastuzumab-resistant HER2-positive breast cancer. Further studies are now needed to assess the value of this approach in clinical practice.

Keywords

Nanobody; Photodynamic therapy; Fluorescence imaging; HER2-positive breast cancer; Trastuzumab-resistant

1 Introduction

Breast cancer is one of the most common cancers in women worldwide. Despite increased understanding of its development and progression, as well as advances in the development of novel therapeutic strategies, breast cancer remains a clinical challenge. Human epidermal growth factor receptor-2 (HER2) is overexpressed in 15–20% of breast cancer patients, and results in a more aggressive disease with a greater likelihood of recurrence [1,2]. In 1998, trastuzumab was introduced as the targeted therapy for HER2-positive cancers. Trastuzumab is a recombinant, humanized monoclonal antibody, which recognizes an epitope on subdomain 4 of HER2 extracellular domain [3].

At present, HER2-positive breast cancer is treated with HER2 blockade, such as trastuzumab, in the neoadjuvant, adjuvant, and metastatic setting. Although the use of trastuzumab led to significant reduction of recurrence and mortality in HER2-positive breast cancer patients [1,4], a substantial number of patients still had residual disease after neoadjuvant therapy leading to a worse prognosis compared to those who have no residual cancer [5–7]. Approximately a quarter of patients who receive treatment for early breast cancer remain at risk of relapse after 8–10 years, and around 15% of these patients will die within a decade [8–10]. In addition, a significant number of patients with HER2 overexpressing metastatic breast cancer are or will become resistant to anti-HER2-based

therapy with trastuzumab [11,12]. Patients with previously treated HER2-positive breast cancer have been shown to benefit from new anti-HER2 therapies, as pertuzumab, lapatinib, or the antibody-drug conjugate trastuzumab-emtansine [13–17], suggesting that other drugs targeting HER2 might provide trastuzumab-resistant patients with additional clinical benefit. In an attempt to develop an additional treatment for HER2-positive breast cancer patients, and in particular for trastuzumab-resistant patients, we have investigated a targeted form of photodynamic therapy.

Photodynamic therapy (PDT) has been employed in the clinic for treatment of a range of cancers (*e.g.* skin, lung, bladder, head and neck, and very recently primary breast cancer [18] and non-oncological disorders (*e.g.* antimicrobial PDT, age-related macular degeneration) [19]. PDT relies on the photosensitizing properties of a chemical compound, *i.e.* a photosensitizer (PS), combined with light of a specific wavelength, and oxygen present in close proximity to the PS. The PS exposure to light converts nearby oxygen into singlet oxygen [20,21] and other reactive oxygen species (ROS) which induce direct cellular damage, resulting in cancer cell death *via* a variety of mechanisms that include apoptosis and necrosis [20]. In addition, impairment of tumor-associated vasculature and an immune response against cancer cells, also contribute to tumor regression. Even though the activation of the PS occurs locally, only where light is applied, the fact that conventional PS are hydrophobic, and non-selective molecules, makes PDT often associated with damage to surrounding normal tissue and unwanted skin phototoxicity. The conjugation of more hydrophylic PS to conventional monoclonal antibodies is currently being tested in the clinic and reduces these unwanted effects, by specifically targeting the PS to cancer cells [22,23].

Recently, we have been investigating an alternative approach for targeted PDT, in which we conjugate the same PS as currently being tested in the clinic (*i.e.* IRDye700DX) to nanobodies [24–28]. Nanobodies are the smallest naturally occurring, functional antigen binding fragments of only 15 kDa, derived from heavy-chain only antibodies present in *Camelidae* [29]. The advantage of nanobodies lies in the combination of their small molecular size, with high binding affinity for their targets. Such combination of features of labeled nanobodies results in high accumulation at the tumor site, better tumor penetration and faster clearance from blood-circulation, as shown in a number of cancer imaging studies [30–37], including HER2-positive breast cancer tumors [38–42]. We therefore anticipate that, in the clinic, PDT employing nanobodies will lead to decreased skin and normal tissue phototoxicity and will allow light application more rapidly after PS administration (hours instead of days for antibody-based PS conjugates).

To date, we have shown that nanobody-PS conjugates bind selectively to their target and upon illumination are able to induce selective cell killing *in vitro*, in particular in cells overexpressing the target of interest, such as EGFR [24,25], c-MET [26] or US28 [27], while not affecting the low/negative or normal cells. *In vivo*, EGFR-targeted PDT has shown to induce extensive tumor damage, as observed on tissue sections processed from orthotopic tongue tumors collected 24 h post PDT [25]. In addition, an intravital microscopy study has confirmed that besides the direct damage to tumor cells, vascular effects are also triggered by nanobody-targeted PDT [28]. These encouraging results stimulated further research to

assess, for the first time, the effect of nanobody-targeted PDT on tumor growth over a month post therapy.

In this study, we have selected and characterized two monovalent nanobodies (1D5 and 18A12) specifically targeting HER2, and have constructed a biparatopic nanobody (1D5-18A12), to facilitate PS internalization as described previously [24,43]. The two most promising nanobodies (1D5 and 1D5-18A12) were then conjugated to the traceable PS IRDye700DX, characterized *in vitro* and evaluated in nanobody-targeted PDT for both trastuzumab-sensitive and -resistant breast cancer cells. Next, two orthotopic breast cancer models were employed: HCC1954, which is a trastuzumab-resistant HER2 overexpressing model, and MCF-7, a low HER2 expressing model. Quantitative fluorescence spectroscopy was employed to follow the local pharmacokinetics of the fluorescent nanobody-PS conjugates, in order to determine the optimal time-point for illumination. This was combined with optical imaging to verify the accumulation of nanobody-PS conjugates in tumors. Finally, the efficacy of nanobody-targeted PDT was evaluated in both models by following tumor growth for 30 days after treatment.

2 Materials & methods

2.1 Phage display selection and production of anti-HER2 nanobodies

To select nanobodies specifically binding to human HER2 receptor, two different and previously described phage display libraries were panned on captured HER2 extracellular domain (MCF7L1 and BT474L1) [44,45]. Briefly, anti-HER2 phages were selected on recombinant purified HER2-ECD containing a Fc tail, captured on a Maxisorp plate (Nunc, Rochester, MN, USA) *via* rabbit-anti-human IgG antibody (DakoCytomation, Glostrup, Denmark). Coated wells were blocked with 4% milk powder in PBS for 1 h at room temperature (RT). Phages pre-blocked with 4% milk-powder for 30 min at RT were panned for binding to immobilized HER2-ECD. After extensive washing with PBS/0.05% Tween-20, phages were eluted with trypsin (Sigma-Aldrich, Saint Louis, MO, USA). The coding sequences of the obtained nanobodies binding to the HER2 ectodomain were identified by performing sequence analysis (Macrogen Inc., The Netherlands).

From these selections, two distinct nanobodies targeting HER2, namely 1D5 and 18A12, were identified and employed in this study. From the two nanobodies, a bivalent nanobody, *i.e.* 1D5-18A12, was constructed as nanobody-encoding genes were PCR amplified using the Expand High Fidelity PCR System (Roche, Mannheim, Germany) with an appropriate primer set, purified, cut with restriction enzymes, and cloned into Sfi1-*Bst*EII cut pET28A vector. Linker sequence (composed of two Gly4-Ser (G4S) repeats) was encoded in the primers. Constructs were sequenced to verify that no mutations were introduced by PCR. These nanobodies were produced in *E. coli* and purified through immobilized metal affinity chromatography (IMAC) as described previously [45].

2.2 Cell lines and culture conditions

Several human breast cancer cell lines were employed, which differ in HER2 expression level and are either responsive or resistant to trastuzumab treatment. HER2-positive breast

cancer cell line SKBr3, which is sensitive to trastuzumab treatment, and the HCC1419, HCC1954, and JIMT1 cell lines, which are resistant to trastuzumab treatment were employed. As control, the low HER2 expressing cancer cell line MCF-7 and HER2-negative breast cancer cell line MDA-MB-231 were employed. JIMT1 cells were purchased from DMSZ (DSMZ GmbH, Germany) and all other cell lines from the American Type Culture Collection (ATCC, Manassas, VA, USA). All cells, except from HCC1419 and HCC1954 cells, were cultured in DMEM (Gibco) supplemented with 7.5% (*v*/v) FBS, 100 IU/ml penicillin, 100 mg/ml streptomycin, and 2 mM L-glutamine. HCC1419 and HCC1954 cells were maintained in RPMI medium supplemented as described above.

2.3 Immunofluorescence

Two hundred thousand HER2 high or HER2 low expressing cells were grown on coverslips for 2 days. On the day of the assay, cells were washed with CO_2-independent medium and incubated for 1.5 h at 4 °C with a 50 nM solution of a nanobody (namely 1D5, 18A12, 1D5-18A12). Unbound nanobodies were removed and cells were fixed with 4% paraformaldehyde (PFA). Bound nanobody was detected with rabbit anti-VHH K1219 (1:1000 for 1 h at RT) (QVQ, Utrecht, The Netherlands), followed by goat anti-rabbit Alexa 488 (1:1000 for 1 h at RT) (Invitrogen, Breda, The Netherlands). Cell nuclei were stained with DAPI (Roche, Almere, The Netherlands). Images were acquired using a confocal laser scanning microscope LSM700 (Carl Zeiss Microscopy GmbH) with a x63 oil objective (Plan-Apochromat 63×/1.40 Oil DIC M27). Of note, difficulties in observing the individual cellular memembranes were occasionally noticed, in particular for HCC1914, which was attributed to more pronounced rounded morphology of cells that coincided with rapid detachment of these cells.

2.4 Determination of apparent affinity of nanobodies on HER2-positive cells

Binding studies were performed with the nanobodies on a panel of HER2 expressing cells: SKBr3, HCC1954, JIMT1 and MCF-7 cells. The HER2-negative cell line MDA-MB-231 was employed as control. Twenty thousand cells were seeded per well 2 days in advance in 96-well plates. Cells were incubated at 4 °C for 1.5 h with a dilution series of nanobodies in DMEM without phenol red, supplemented with 25 mM HEPES and 1% BSA, pH 7.2 (binding buffer). Nanobodies were added in a concentration range from 0.48 nM to 500 nM. After several washes cells were fixed with 4% PFA for 30 min at RT and the fixative was quenched by 10 min incubation with 100 mM glycine in PBS. The detection of bound nanobodies was performed with the use of rabbit anti-VHH protein G purified serum (1:1000 for 1 h at RT), followed by a goat anti rabbit-IRDye800CW (1:1000 for 1 h at RT). The fluorescence signal was detected using the 800 nm channel of the Odyssey scanner (LI-COR Biosciences, Lincoln, NE, USA).

2.5 Conjugation of the PS IRDye700DX to the nanobodies and their binding affinities

The two HER2-targeted nanobodies displaying the highest affinity were randomly conjugated to the IRDye700DX (PS) (LI-COR Biosciences) through an N-hydroxysuccinimidine (NHS) ester by coupling to the primary amines of the nanobodies (*i.e.* N-terminal amino acid and lysine residues) as described before [24]. Conjugation of the PS was performed with a four-fold molar excess of PS for the monovalent nanobody and two-

fold molar excess for the bivalent nanobody for 2 h at RT. After conjugation, the unconjugated PS was removed using sequentially two (in case of 1D5-18A12) or three (in case of 1D5) Pierce ZebaTM Desalting Spin Columns. The degree of conjugation (DoC) was determined according to the instructions given by the provider of the PS. The obtained PS conjugated nanobodies are referred to as nanobody-PS (1D5-PS and 1D5-18A12-PS).

As random conjugation can have a detrimental effect on binding properties of nanobodies [46], the apparent affinities of 1D5-PS and 1D5-18A12-PS were determined in binding studies on SKBr3, HCC1954, and MDA-MB-231 cells. For this, the assay was performed as described for the nanobodies except that the cell bound nanobody-PS conjugates were detected directly through the PS fluorescence, after the washing steps, using the 700 nm channel of the Odyssey scanner.

2.6 In vitro photodynamic therapy

One day after seeding 20.000 cells per well in 96-well plate (Greiner Bio-One, Alphen a/d Rijn, The Netherlands), cells were washed with DMEM without phenol red supplemented with 7.5% (v/v) fetal bovine serum (FBS), 100 IU/ml penicillin, 100 mg/ml streptomycin and 2 mM L-glutamine (referred as PDT medium). Then cells were incubated with a dilution series of nanobody-PS conjugates for 30 min at 37 °C (short incubation time aimed to reflect nanobodies' short half-life). After the incubation cells were washed twice with the PDT medium and the detection of total fluorescence (*i.e.* bound and internalized fluorescence of the nanobody-PS conjugates) was performed immediately afterwards using the Odyssey scanner. Thereafter, cells were illuminated for 42 min with 4 $mW \cdot cm^{-2}$ fluence rate for a total light dose of 10 $J \cdot cm^{-2}$, using a custom-made device consisting of 96 LED lamps (670 ±10 nm, 1 LED per well), connected to a water bath thermostated at 37 °C. An Orion Laser power/energy monitor (Ophir Optronics LTD, Jerusalem, Israel) was used to measure and adjust the light intensity. After illumination, cells were placed back in an incubator. In all experiments, an internal negative control was included (those cells were not subjected to illumination). Experiments were repeated at least twice.

2.7 Cell viability assay

After an overnight post treatment incubation, cells were incubated with Alamar Blue Reagent, according to the manufacturer's protocol (AbD Serotec, Oxford, United Kingdom). The fluorescence was detected with a Fluorostar 2 h after addition of the reagent. Results are expressed as cell viability in percentage (%), relatively to the untreated cells. The concentration of nanobody-PS conjugates subjected to illumination and leading to 50% lethal dose (LD_{50}) was determined using the GraphPad Prism 5.02 software (GraphPad Software, San Diego, CA, USA).

2.8 Imaging of apoptotic and necrotic cells

Cellular morphology was assessed and apoptotic and necrotic cells were distinguished with Annexin V-FITC and propidium iodide (PI) staining, at different time points post illumination. HER2-positive (HCC1954) and HER2 low expressing (MCF-7) cells were seeded in 96-wells plates one day before the incubation with 25 nM nanobody-PS followed by illumination (10 $J \cdot cm^{-2}$ of light dose). Apoptotic cells were detected with Annexin V-

FITC (BioLegend, San Diego, CA, USA), whereas necrotic cells were detected with PI (Invitrogen), either 1 h or 24 h after light application. Cells were incubated with 10 μM Staurosporine (Sigma-Aldrich) for 24 h as a control for apoptotic cell death, while 1% Triton X-100 (Sigma-Aldrich) was incubated with cells for 3 h to permeabilize cells, mimicking necrosis. Images were taken using the bright field, GFP and RFP channels on the EVOS Microscope (Advanced Microscopy Group, AMG, Thermo Fischer Scientific) equipped with 10× objective (Plan Fluor, 10×, NA 0.3, Air and working distance 8.3 mm, AMG) as described before [24].

2.9 Animal model

Nude CD-1 (Crl:CD1-Foxn1^{nu}) female mice (Charles River laboratories, l'Arbresle, France), aged 4–6 weeks, were housed in individually ventilated cages and provided with food and sterilized water *ad libitium*. Animal experiments were approved by the local animal welfare committee of the Leiden University Medical Center. Under general anesthesia, a small incision between the fourth and fifth nipple was made, bilaterally. The mammary fat pads were exposed and subsequently 3×10^6 HCC1954 cells (high HER2 expressing and trastuzumab-resistant) or 0.5×10^6 MCF-7 cells (low HER2 expressing), were injected in a 30 μl volume (PBS) into the mammary gland bilaterally. Thereafter, the skin was closed with sutures. General animal health was checked three times a week by weight measurements and inspection of the abdomen. Tumor growth was monitored three times a week by measurement with digital calipers and tumor volume (mm^3) was determined with the formula length × width^2 × 0.52. Experiments were started when the tumors reached a volume of approximately 100–130 mm^3 and the treatment volume was defined 100%.

2.10 Quantitative fluorescence spectroscopy in vivo

To determine the optimal time point for illumination, quantitative fluorescence spectroscopy was performed as described previously [25,47]. Mice were randomly divided into two groups and received 100 μg of 1D5-PS intravenously. After verifying 1D5-PS accumulation in HER2 overexpressing tumors, only mice with HCC1954 tumors received 200 μg of 1D5-18A12-PS (all groups consisting of 2–3 mice, each mouse receiving approximately 6 nmol of PS to allow comparison). Quantitative fluorescence spectroscopy measurements were performed 0.5, 1, 2 and 4 h after injection of the conjugates under isoflurane anesthesia. The tumor was exposed by a small incision in the inguinal skin. Care was taken to position the fiber probe on the tumor. Between measurements the skin was closed with sutures. Measurements were performed in triplicate on the tumor, ipsilateral normal mammary gland (behind the second nipple), and skin. The resulting intrinsic fluorescence signals, expressed as $Q \cdot \mu_{a,x}^{f}$ where Q is the fluorescence quantum yield of the conjugate, was statistically analyzed using the GraphPad Prism 5.02 software. Analysis of significance was performed by unpaired Student's *t*-test and differences with *p*-values < .05 were considered significant.

2.11 In vivo optical imaging and photodynamic therapy

Mice were divided in three groups for each tumor model, receiving in 100 μl of PBS in the tail vein: a. 100 μg 1D5-PS (n = 8 HCC1954, n = 7 MCF-7), b. 200 μg 1D5-18A12-PS (n =

13 HCC1954, n = 6 MCF-7), or c. vehicle as control (n = 11 HCC1954, n = 9 MCF-7), including tumors exposed to illumination only (n = 2 HCC1954, n = 1 MCF-7). Fifteen minutes before illumination, and under anesthesia with isoflurane, optical imaging of the fluorescence of the nanobody-PS conjugates was performed with the Pearl Trilogy Small Animal Imaging System (LI-COR Biosciences) to access the accumulation of the nanobody-PS in both tumor models.

Subsequently, at the best time point selected through quantitative fluorescence spectroscopy, mice were brought in a dark room, under isoflurane anesthesia and received a subcutaneous injection of a painkiller. The area surrounding the tumor was covered with black paper to protect the animal from any scattered laser light. The unilaterally breast tumors were then illuminated using a 690 nm diode laser (Modulight, Tampere, Finland). The power at the end of the optic fiber was calibrated with a power meter (Gigahertz optic, Turkenfield, Germany). Light was delivered *via* a 600 μm optic fiber with a fluence rate of 50 $mW \cdot cm^{-2}$. The exposure time was adjusted to obtain a fluence of 100 $J \cdot cm^{-2}$. Tumor growth was measured with a caliper, three times a week, until 30 days after treatment or until the (contralateral) tumor reached the maximum size of 750 mm^3. Mice were sacrificed by induction of anesthesia with isoflurane followed by cervical dislocation.

2.12 Tumor volume and statistical analysis

Tumor volume values are expressed as means±standard deviation (SD). The short term effect of PDT was evaluated 3 days after illumination. The regression and/or growth of the tumor at the long term after PDT was determined by linearly interpolating the points in time at which the tumor reached a volume of respectively 50, 100, 200, 300, 400 and 500% using the equation $y = A.e^{(b.x)}$ where, before treatment, A, is the size of the tumor at day 0 (set to 100%) and b is the tumor growth rate. After the treatment, A, can be related to the fraction of cells that survive PDT. The effectiveness of the treatment was determined by comparing the mean volume doubling time (time to grow to 200%) and the time to regrow to 100%. The percentage of tumors that have not doubled in volume (tumors not reaching 200% of their original volume 30 days after PDT) was determined and analyzed by a Kaplan-Meier survival curve. Data was statistically analyzed using the GraphPad Prism 5.02 software for Windows (GraphPad Software, San Diego, CA, USA). Analysis of significance was performed by Student's *t*-test (between 2 treatment groups) and one-way ANOVA (for> 2 treatment groups) and differences with *p*-values < .05 were considered significant.

3 Results

3.1 Selected nanobodies bind specifically and with high affinity to HER2

Two nanobodies that bind to HER2 were selected and further characterized: 1D5 from the MCF7L1 immune library and 18A12 from the BT474L1 immune library. These two nanobodies were further engineered into a biparatopic nanobody, 1D5-18A12 (Fig. S1A). The aim of developing a biparatopic nanobody was to favor the accumulation of the photosensitizer inside the cell, as previously observed with other nanobody-photosensitizer conjugates [23]. To demonstrate that the selected nanobodies recognize non-overlappiong epitopes, a competition assay was performed. As the excess of one of them did not affect the

binding of the other phage, we conclude that the two nanobodies bind non-overlapping epitopes and can be used for producing a biparatopic anti-HER2 nanobody (Fig. S1B).

A panel of breast cancer cell lines was assembled which varied in HER2 expression and sensitivity to trastuzumab. SKBr3, HCC1954 and HCC1419 are high HER2 expressing cells, JIMT1 and MCF-7 have a low HER2 expression level, and MDA-MB-231 cells are considered negative for HER2 expression (Fig. S2AB). Of these, only SKBr3 cells are sensitive to trastuzumab treatment (Fig. S2C). The binding specificity of the three nanobodies was observed by immunofluorescence with a clear fluorescent signal at the cell membrane of cells highly expressing HER2, namely SKBr3, HCC1419 and HCC1954, whereas a very faint fluorescence signal was detected for all nanobodies on MCF-7 cells, and almost no fluorescence signal on JIMT1 cells (Fig. 1A). These nanobodies do not compete for the binding epitope with trastuzumab (data not shown).

Very high binding affinities to HER2-positive cells were observed for the three nanobodies: for 1D5 affinities of 4.1 ± 1.7 nM in SKBr3 cells and 2.1 ± 0.4 nM in HCC1954 cells were observed, whereas for 18A12 a slightly lower affinity was observed: 11.5 ± 4.0 nM in SKBr3 cells and 16.7 ± 4.9 nM in HCC1954 cells, respectively (Fig. 1B). A high affinity was also obtained for the biparatopic nanobody: 3.1 ± 0.6 nM in SKBr3 cells and 4.6 ± 0.6 nM in HCC1954 cells. Importantly, no binding was detected to the HER2-negative MDA-MB-231 cells, not even at the highest concentrations of 500 nM, which demonstrates specific binding to HER2. To JIMT1 and MCF-7 cells only very low binding was observed with the biparatopic nanobody, which correlates with the low HER2 expression level (Fig. S2B). The differences in the extent of maximum binding (B_{max}) between HCC1954 and SKBr3 likely reflect differences in epitope availability, as the HER2 expression determined by western blotting was only slightly higher in HCC1954 cells (Fig. S2B).

Internalization of these HER2-targeting nanobodies was assessed using radio-labeled nanobodies incubated with SKBr3 cells as described previously [43]. The 18A12 nanobody showed a slightly higher internalization rate constant (k_e), as compared to 1D5, while the biparatopic nanobody 1D5-18A12 showed a ten-fold increase in internalization, compared to 1D5 (Fig. S3). These results are in agreement with previous results using biparatopic anti-EGFR nanobodies [43]. The electron microscopy data further supports the internalization of both 1D5 and 1D5-18A12 nanobody (Fig. S4).

3.2 Nanobody-PS conjugates retain their binding properties

The photosensitizer IRDye700DX (PS) was subsequently conjugated to 1D5 and 1D5-18A12. The success of conjugation was examined by SDS-PAGE, which also showed the remaining free PS. All nanobody-PS preparations contained less than 10% of free PS (Fig. S5A). The degree of conjugation (DoC) was close to one for both nanobody-PS conjugates and this process was reproducible. The apparent binding affinities (K_D) of both 1D5-PS and 1D5-18A12-PS were only slightly affected, with values of: 8.2 ± 0.9 nM and 7.8 ± 0.9 nM on SKBr3 cells, and 5.4 ± 0.9 nM and 10.1 ± 1.1 nM on HCC1954 cells, respectively (Fig. 2A). Overall, both nanobody-PS conjugates remained able to bind with low nanomolar affinities to HER2 present on trastuzumab-sensitive cells (SKBr3 cells), and

on trastuzumab-resistant cells (HCC1954), while no binding was observed to the negative cells (MDA-MB-231), which correlates with expression levels of HER2 (Fig. S2B).

3.3 Nanobody-PS conjugates are potent and selective PDT agents

The association of the conjugates with the different cell lines at 37 °C also correlated well with their HER2 expression level (Fig. 2B). After illumination for PS activation, both nanobody-PS showed to be very potent and capable of inducing cell death, specifically on cell lines with high HER2 expression. The LD_{50} of 1D5-18A12-PS determined on SKBr3 cells was 3.1 ± 1.7 nM, on HCC1954 1.8 ± 1.5 nM and on HCC1419 1.7 ± 0.5 nM (Fig. 2C). Interestingly, for 1D5-PS, the LD_{50} determined was 2 to 3 times higher than for 1D5-18A12-PS: on SKBr3 cells LD_{50} was 7.2 ± 3.4 nM, on HCC1954 5.5 ± 1.9 nM, and on HCC1419 4.7 ± 0.9 nM (Fig. 2C). Notably, both nanobody-PS caused no toxicity on low HER2 expressing MCF-7 cells, which was in agreement with binding assays (Fig. 1B) and incubation data (Fig. 2B), and confirmed the selectivity of nanobody-targeted PDT. Moreover, as we have clearly demonstrated in previous studies [24,25], nanobodies alone, PS alone, or nanobody-PS without illumination had no effect on the viability of SKBr3 and HCC1954 cells (Fig. S5B). In addition, toxicicty could be reduced by sodium azide, a singlet oxygen quencher (data not shown).

For both 1D5-PS and 1D5-18A12-PS, as early as 1 h after illumination, some cell damage was observed in phase contrast images, which was accompanied with PI staining of a fraction of HCC1954, suggesting necrosis. The toxic effect increased with time, as shown by the increase of PI staining at 24 h compared to 1 h post illumination (Fig. 3). The majority of cells were also positive for Annexin-V, indicating apoptosis, although the rapid and concomitant staining with PI suggests necrosis. In addition, there is a clear difference in morphology of cells that are only undergoing apoptosis (Staurosporine control), compared to the effect induced by nanobody-targeted PDT.

3.4 Quantitative fluorescence spectroscopy and optical imaging show specific accumulation of nanobody-PS conjugates in high HER2 expressing tumors

Inoculation with either HCC1954 cells or MCF-7 cells led to the development of orthotopic breast tumor models with high and low HER2 expression, respectively, as confirmed through histological assessment (Fig. S6A).

Both nanobody-PS conjugates were found in a higher degree in HCC1954 tumors compared to the ipsilateral mammary gland (without tumor) and skin, verifying the tumor specificity of these conjugates (Fig. 4A). Differences in quantitative fluorescence between tumor and normal mammary gland were statistically significant ($p < .05$) at time point 1 h post injection for both nanobody-PS (respectively tumor *vs* mammary gland 1D5-PS: $Q \cdot \mu_{a,x}^{f} = 3.24 \times 10^{-3}$ *vs* 1.40×10^{-3} and $Q \cdot \mu_{a,x}^{f}$ = 18A12-PS: 2.35×10^{-3} *vs* 1.20×10^{-3}) and at 2 h post injection only for 1D5-PS (tumor *vs* mammary gland 3.56×10^{-3} *vs* 1.83×10^{-3}). At 1 and 2 h after injection, there was no significant difference between quantitative fluorescence of 1D5-PS and 1D5-18A12-PS present in HCC1954 tumors. Importantly, the quantitative fluorescence of 1D5-PS and 1D5-18A12-PS at 2 h post injection was significantly higher in HCC1954 tumors than that of 1D5-PS in MCF-7 tumors (3.07×10^{-4}, respectively $p < .001$

and $p < .05$), verifying the selectivity of these conjugates to high HER2 expressing tumors. The maximum quantitative fluorescence of 1D5-PS and 1D5-18A12-PS was observed at 2 h post injection, after which the intrinsic fluorescence decreased. No significant differences were observed in normal skin tissue between 1D5-PS conjugates in HCC1954 and MCF-7 tumors. Based on these quantitative fluorescence spectroscopy measurements, 2 h post injection was the time point chosen to apply light for PDT.

Optical imaging at 700 nm performed 15 min before the illumination time point also confirmed the accumulation of 1D5-PS and 1D5-18A12-PS in the high HER2 expressing model (Fig. 4B). In contrast, in the low HER2 expressing tumors no or clearly less accumulation of either nanobody-PS conjugates was observed. In addition, fluorescence was non-invasively detected in the kidneys, bladder, and liver. Although no biodistribution study was here conducted, the presence of fluorescence in these organs was expected, based on previous biodistribution studies with nanobodies [45]. Together, the quantitative fluorescence spectroscopy and optical imaging showed that the conjugates accumulate specifically in the high HER2 expressing breast tumor model.

3.5 Nanobody-targeted PDT induces tumor regression of high HER2 expressing breast tumors after a single treatment session

The average size of HCC1954 tumors at the day of PDT (day 0) was 93 ± 20 mm^3 (1D5-PS) and 142 ± 21 mm^3 (1D5-18A12-PS), for MCF-7 tumors the average size was and 128 ± 7 mm^3 (1D5-PS) and 153 ± 58 mm^3 (1D5-18A12-PS). The average tumor size of HCC1954 tumors treated with 1D5-PS PDT were somewhat smaller than HCC1954 tumors treated with 1D5-18A12-PS PDT ($p < .05$). An overview of the treatment schedule is represented in Fig. 5A. Skin lesions with scarring, edema or necrosis were seen 2 days after PDT in mice treated with 1D5-PS and 1D5-18A12-PS and illumination and at location of HCC9154 and MCF-7 tumors. These lesions were all self-limiting one week after PDT. Besides skin lesions, no other side effects of PDT were seen.

The high expressing HER2 tumors (HCC1954) showed a significant tumor volume reduction after both nanobody-PS mediated PDT treatments, compared to control tumors ($p < .001$), which was not significantly different for the two nanobody-PS conjugates investigated ($p = .65$) (Fig. 5B). Three days post treatment the tumor volume was reduced to 27.2% ± 14.5 for 1D5-PS and 50.1% ± 24.9 for 1D5-18A12-PS mediated PDT, whereas the control showed growth to 112.8% ± 4.2. These results are supported by the decreased cell proliferation observed 24 h post PDT, through the low intensity of Ki67 staining, compared to the control (Fig. S7). Control HCC1954 tumors, receiving no nanobody-PS or light, showed a mean volume doubling time of 19 ± 6 days. After 1D5-PS mediated PDT only 1 out of 7 tumors (14%) grew back to more than 100% and growth was delayed by 22 days (Fig. 5C). While the tumor in the other 6 animals did not reach 100%, tumor growth was delayed by more than 30 days. After 1D5-18A12-PS mediated PDT, 5 out of 12 tumors (42%) grew back to 100% within 21 ± 7 days. The growth of the tumor in the other 7 animals did not reach 100%, and the tumor growth was delayed by more than 30 days. The follow-up of four mice with a HCC1954 tumor (treated with 1D5-PS PDT; n = 3 and

1D5-18A12-PS PDT; n = 1) was shorter than 30 days due to a maximum tumor size on the contralateral side (Fig. 5C).

The low HER2 expressing tumor model showed no regression of tumor volume after nanobody-targeted PDT (Fig. 5B). The mean tumor volume at day 3 after PDT was 111.9% ± 19.0 after 1D5-PS and 114.7% ± 13.4 after 1D5-18A12-PS mediated PDT compared to 145% ± 12.1 for the controls. These results are also supported by the decreased cell proliferation observed through low intensity of Ki67 staining, 24 h post PDT compared to the control group (Fig. S7). Notably, after day 3, tumor growth resumed at a similar rate as the untreated tumors. The growth of MCF-7 tumors injected with 1D5-PS or 1D5-18A12-PS followed by illumination, was not significantly different from the tumors in their control group ($p = .13$). Control MCF-7 tumors, receiving no nanobody or light, showed a mean volume doubling time of 6 ± 1 days. After 1D5-PS mediated PDT the mean volume doubling time was 8 ± 2 days compared to 9 ± 3 days after 1D5-18A12-PS mediated PDT (Fig. 5C).

4 Discussion

The aim of this study was to investigate an alternative treatment option for breast cancer patients, in particular trastuzumab-resistant cancers. For that we have developed nanobody-PS conjugates targeting HER2 that are capable of binding specifically and with high affinities to this receptor on both trastuzumab-sensitive and -resistant cell lines. Upon illumination of nanobody-PS associated with cells, selective cytotoxicity was induced in HER2 overexpressing cells, whereas the HER2 low expressing cells remained unaffected. Quantitative fluorescence spectroscopy and optical imaging confirmed that the nanobody-PS accumulate specifically in the high HER2 expressing breast tumor model, and indicated 2 h post injection as most suitable time point for illumination. Importantly, the efficacy of nanobody-based PDT was confirmed *in vivo*, where significant tumor regression was observed for the high HER2 expressing tumors, while only a slight growth delay of 2–3 days was induced in the low HER2 expressing tumors. In fact, at day 3 after PDT mediated with 1D5-PS, HCC1954 tumor sizes were reduced to a third of their original size, and 6 out of 7 tumors did not regrow. Considering this significant tumor regression was induced in the high HER2 expressing model after a single treatment only, the present study demonstrates not only the selectivity, but also the potency of nanobody-targeted PDT.

To our knowledge, this is the first study in which the potential of HER2-targeted PDT was evaluated for treatment of both trastuzumab-sensitive and trastuzumab-resistant breast cancer cells. Our *in vitro* results, conducted with a panel of different breast cancer cell lines, showed that nanobody-targeted PDT is potent and selective. Other approaches have been investigated for targeted PDT in breast cancer. In comparison to using peptide-based factor VII-targeted veterpforin PDT of breast cancer cells, nanobody-targeted PDT showed efficacy (LD_{50}) at 1000-fold lower concentration, even with a six times lower total light dose [48,49]. Stuchinskaya et al. and Obaid et al. have also shown a significantly decreased viability of HER2 overexpressing SKBr3 cells after treatment with anti-HER2 antibody conjugated gold nanoparticles and irradiation [50,51]. However, this was reached with still 40% of the cells remaining alive (with the same conditions as light dose and conjugate

concentration as the present study) [50] or a 10 to 100 fold higher concentration of the PS conjugates [51]. Although a comparison to other targeted PDT of breast cancer cells is difficult due to difference in the setting of experiments, including cell conditions, the differences in LD_{50} after nanobody-based PDT are encouraging.

We have previously shown that internalizing nanobodies are more effective in *in vitro* PDT assays than the nanobodies that remain at the cell surface [23], which is also in line with other reports using internalizing *versus* non-internalizing antibody-PS conjugates [47–49]. Internalization of PS was achieved by employing a biparatopic nanobody, which is known to promote receptor-mediated internalization [43,50]. The bivalent nanobody-PS in this study was verified to be biparatopic and, led to a higher internalization rate constant of the HER2, in comparison to a monovalent counterpart (Fig. S3). Even though the biparatopic format was more effective *in vitro*, *i.e.* lead to 2–3 times lower LD_{50}, no significant differences between 1D5-PS and 1D5-18A12-PS mediated PDT were observed when treated cells were exposed to Annexin-V or propidium iodide staining. The rapid damage observed combined with propidium iodide staining suggests necrosis, although the majority of cells appear positive for Annexin-V (Fig. 3). We however cannot exclude, other mechanisms of cell death following nanobody-targeted PDT. Furthermore, the damage inflicted on the cell membrane upon illumination could possibly expose phosphatidylserine, thereby leading to Annexin-V staining, without necessarily triggering apoptotic cell death. Consequently, no quantification of necrotic or apoptotic cells was attemped in the present study and the emphasis was directed to the observation of mixed events.

The optimal time interval for illumination was determined by quantitative *in vivo* fluorescence spectroscopy which determines the intrinsic fluorescence corrected for the influence of tissue optical properties [47]. Quantitative spectroscopy showed the highest uptake of nanobody-PS in high HER2 expressing tumors and not in the normal mammary gland, in the skin, nor in the low HER2 expressing tumors, supporting tumor-cell association of the conjugates, rather than presence in the vasculature (*i.e.* bloodstream). It is important to note that fiber optic spectroscopy does not reveal information on the cellular distribution of PS and is unable to effectively monitor the microscopic vasculature *in vivo*. Although we have not yet conducted intravital microscopy studies with the breast cancer model presented here, we can expect some association of the conjugates with the vasculature of the tumors, as we recently observed for nanobodies targeting EGFR [52]. Nevertheless, this association is likely not pronounced as no significant accumulation at the tumor was observed for the low HER2 expressing model, either through fluorescence spectroscopy (Fig. 4A) or non-invasive imaging with the Pearl Imaging System (Fig. 4B). Although no further quantitative biodistribution was performed in this study, the fluorescence detected in kidneys, bladder and liver correlates with the biodistribution profile of other near-infrared-labeled nanobodies [45,53].

The highest intrinsic fluorescence in HER2-positive tumors was obtained with 1D5-PS, demonstrating 1D5-PS as the leading nanobody to carry PS to the tumor. In our previous nanobody-targeted PDT study, the monovalent and biparatopic nanobody were administrated in equal amounts (micrograms) of nanobody and equal molar amounts of PS, but with a difference in degree of conjugation (thus, twice as many molecules of monovalent compared

to biparatopic nanobody). This resulted in an approximately 2-fold difference in fluorescence intensity in favor of the biparatopic nanobody-PS [25]. As the degree of conjugation of the monovalent and biparatopic nanobody-PS was the same in the present study (allowing the injection of the same number of molecules of monovalent and biparatopic nanobody, although different amounts in μg), the smaller size of the monovalent nanobody-PS possibly led to a better distribution within the tumor [54], thus resulting in higher intrinsic fluorescence values. It is well recognized that the actual amount of PS in the tissue predominantly determines the phototoxic effect. Therefore, local illumination at the tumor was applied 2 h post injection of the nanobody-PS conjugates, when the concentration of the PS was at maximum. After PDT, to a dose of 100 $J \cdot cm^{-2}$ at 50 $mW \cdot cm^{-2}$ we observed IRDye700DX photobleaching, as there was clearly less fluorescence seen with the Pearl Imaging System in the treated tumor in comparison to the non-treated tumor (Fig. S6B). We believe that this is the first report of this effect *in vivo* for IRDye700DX. PS photobleaching during PDT has been extensively investigated for other PS and has been shown in some cases to be useful for monitoring PDT efficacy [55].

Remarkably, single treatment with both nanobody-PS showed a significant regression of high HER2 expressing tumors. There was no significant difference between the regression of these tumors during the 30 days post illumination, when those received either 1D5-PS or 1D5-18A12-PS, although the regression was higher after 1D5-PS PDT. This is consistent with the higher fluorescence intensity of 1D5-PS in HCC1954 tumors, compared to the fluorescence of 1D5-18A12-PS. In contrast, in the low HER2 expressing tumors, only a small growth delay was observed. This short growth arrest is supported by the low Ki67 staining observed 24 h post PDT (Fig. S7). The combination of the presence of low HER2 expression and possible vascular effect of PDT may explain this small effect *in vivo,* where *in vitro* there is no effect on cell viability. The short-term effect of HER2-targeted PDT on low HER2 expressing tumors is suggested to be mild, since these tumors recovered and continued to grow at the similar rate as the non-treated MCF-7 tumors. The expression level of the target, although not the unique factor, as cells can be more or less resistant to reactive oxygen species or more or less protected from apoptosis [56], is certainly critical for the success of the treatment, as already previously suggested [25,26].

In our previous studies, although *in vitro* PDT mediated by biparatopic anti-EGFR nanobody (7D12-9G8-PS) showed a more toxic effect than the monovalent nanobody (7D12-PS), *in vivo* efficacy studies showed a slightly higher phototoxicity induced by the monovalent nanobody-PS conjugates [24]. The present study further supports these observations as the most effective treatment *in vivo* was obtained with the monovalent nanobody-PS, although differences were not significant. This effect is likely due to the fact that, in small monovalent nanobodies, the PS is closer to the cell membrane, and perhaps even more important, it possesses better penetration into the interior of tumors, leading to increased phototoxicity *in vivo* [51]. Thus, while internalization of the PS does not seem to be essential for *in vivo* efficacy, an effective and homogenous tumor distribution of the nanobody-PS conjugate is likely to have a higher impact. Still, we cannot exclude that the better treatment response of the monovalent nanobody-PS is in some extent related to the slightly smaller size of the tumors at the day of treatment. Besides, no therapeutic effect is expected from the

nanobody-PS conjugates alone, considering they are only administered once and have a very short half-live.

Previous *in vivo* HER2-targeted PDT studies have been mainly performed using subcutaneous tumor models (instead of orthotopic models) and antibodies, showing only a restricted growth delay and no regression in size of HER2-positive tumors [57–59]. These studies were performed with comparable amount of antibody-PS (in the range of 100–200 μg) and light dose (100 $J \cdot cm^{-2}$), while using higher fluence rates (150–300 $mW \cdot cm^{-2}$), repetitive drug administration, a longer time period between injection and light illumination of days, and multiple cycles of light illumination. Others achieved significant reduction of tumor volume of HER2-positive gastric cancers (of NCI-N87 and N87-GFP cell lines) with trastuzumab-PS mediated PDT (using the same PS as in our studies) [60,61]. Although no direct comparison was investigated with trastuzumab-PS in our study, the light exposure and PS conjugates conditions in these studies were similar to our study; however, all tumors regrew within 21 days, or light was applied multiple times a week for three weeks. The application of light multiple times over days is clinically not always applicable in patients with breast cancer: the light of a laser has a penetration depth suitable for the illumination of superficial tumors and thus deeper tumors should be exposed during an operation. To further minimize the number of animals used and avoid unnecessary repetitive studies, no control group with trastuzumab alone was included [62]. Considering the previous *in vivo* HER2-targeted PDT studies showing only a restricted growth delay and no regression in size of HER2-positive tumors [59–61,63], the unprecedented results reported in this study are certainly encouraging, as our data show significant tumor regression after a single nanobody-targeted PDT treatment, with a single light application. Yet, it would be interesting to investigate the nanobody-targeted PDT in a more aggressive tumor type.

Furthermore, additional *in vivo* studies which could contribute to an optimized treatment relate to: testing of different light fluences and fluence rates, to minimize side-effects (normal skin damage) even further and possibly enhance efficacy. To explore more about the direct effect of PDT on the vasculature, intravital microscopy imaging could be used to provide longitudinal information on the kinetics and localization of the anti-HER2 nanobody-PS in detail [52]. To investigate complete tumor remission, a longer follow-up of 90 days would be necessary, and, it could also be interesting to investigate our model in immunocompetent mice, as PDT has a strong immune component and the requirement of the immune system for avoiding relapse from cancer is becoming evident [64–67]. Nevertheless, for a more clinically relevant context, nanobody-targeted PDT could be investigated in the postsurgical setting, for HER2-positive breast cancer in primary tumors, which did not respond to neoadjuvant therapy and/or became resistant to trastuzumab, compared to standard clinical treament.

In this study, a human orthotopic tumor model was developd in mice and the used nanobody-PS conjugates do not bind to murine HER2. In humans, normal tissue may also express HER2, which might influence the quality of imaging and the effect of photodynamic therapy. However, only very low expression of HER2 is seen in normal human tissue, whereas HER2-positive breast tumors can have an increase up to 40–100 fold in HER2 protein, resulting in 2 million receptors expressed at the tumor cell surface [68,69]. This

high tumor-to-normal ratio in humans will presumably ensure minimal uptake or effect in benign tissue, which is further warranted by the local illumination necessary to induce cytotoxicity.

Importantly, nanobodies have been approved for clinical use by the European Medicines Agency and recently also by the Food and Drug Administration as antithrombotic agents [44–46]. In oncology, clinical evaluation of nanobodies as imaging agents has been initiated by Keyaerts et al. The ^{68}Ga-HER2 nanobody for PET/CT imaging has shown high tracer accumulation in HER2-positive metastases [34]. Additionally, targeted PDT is currently being investigated in a phase I/ II trial, testing the EGFR-targeted antibody-PS conjugate RM1929, containing cetuximab and IRDye700DX, in patients with recurrent head and neck cancer. RM1929 has been shown to be safe and well tolerated, and promising results with improved complete response and disease control rate were seen (ClinicalTrials.gov Identifer: NCT02422979, data not yet published). One of the major disadvantages of current clinically approved PS is their spectral properties, compelling the PS excitation with light below 660 nm, which results in light penetration of a few millimetres [63,70]. The fluorescent properties of near-infrared IRDye700DX, which allows deeper tissue penetration, makes it a very interesting molecule as it could be employed both for diagnosis and treatment. *In vivo* data already demonstrated that IRDye700DX can safely be used for intraoperative tumor localization using near-infrared imaging [71,72]. In a clinical setting, such nanobody-PS conjugates could be employed first for fluorescence-guided surgery and assist the surgeon in its resection and secondly, upon light exposure of the wound bed, to destroy possible remaining cancer cells and potentially activating the immune system. The decrease in fluorescence of the conjugate can likely be used to monitor the efficacy of PDT and the response of tumors [59]. The fact that both IRDye700DX and nanobodies have already reached the clinic, suggests a smooth translation of nanobody-targeted PDT into clinical practice, to further improve current clinical PDT and provide additional treatment options to HER2-positive, and in particular trastuzumab-resistant patients.

In this study we present a nanobody-based strategy to treat not only trastuzumab-sensitive HER2-positive breast cancer, but also trastuzumab-resistant breast cancer. The mechanisms of resistance to trastuzumab are mostly related to an inactive target receptor by lacking of extracellular binding to domain IV. Binding of other anti-HER2 drugs, as nanobody-drug conjugates, against different epitopes present in the HER2 extracellular domain could provoke an anti-tumor effect in the presence of trastuzumab-resistance. As the HER2 expression levels vary in breast cancer patients, it remains to be elucidated which patients would benefit most from nanobody HER2-targeted PDT. In the clinical setting, HER2-targeted nanobody-PS conjugates could facilitate fluorescence-guided resection and targeted PDT of primary HER2-positive tumors. Intraoperatively, due to chemotherapy-induced fibrosis, it can be difficult to distinguish between tumor or benign tissue and obtain clear resection margins [73,74]. HER2-enriched tumors even have the highest risk of local recurrence after breast-conserving surgery [75,76]. Neoadjuvant systemic chemotherapy plus dual-agent HER2 blockade with complementary mechanisms of action, improved the number of proportion of patients achieving pathological response, however with increased toxicity [10,14]. Anti-HER2 nanobody-targeted PDT could be employed to prevent disease recurrence by optimising the number of HER2-positive early breast cancer patients with no

residual cancer, without imparting toxicity of additional chemotherapy. Also for patients whose tumors are or become resistant to trastuzumab(−based) therapy, anti-HER2 nanobody-targeted PDT could be a viable option. In the particular case of trastuzumab-resistant patients with metastasis, one could foresee the usage of nanobodies targeting HER2 as carriers of drugs or toxic compounds (such as nanobody-drug conjugates) [77–81], although this remains to be further investigated.

The development of combined imaging and therapeutic approaches (designated theranostics) for HER2 overexpressing breast cancer patients is of great importance, as it would simultaneously allow the diagnosis and subsequent treatment of HER2-positive lesions. Furthermore, with HER2 overexpression in many other cancers, including oesophageal, gastric, bladder and endometrial cancers [82,83], our anti-HER2 nanobody-targeted PDT constitutes a promising treatment option to be used across multiple histologically different cancers indications. Especially, for tumors of the gastrointestinal tract where minimally invasive surgery is performed using a laparoscope or endoscope, our nanobody-PS conjugates could provide the opportunity to perform fluorescence imaging and PDT using fiber-optics.

In conclusion, we have developed HER2-targeted nanobody-PS conjugates and for the first time demonstrated significant tumor regression after a single treatment session. Besides combining fluorescence imaging with therapy, this could easily be implemented into current clinical regimens, to successfully treat trastuzumab-resistant and -sensitive HER2-positive breast cancer.

Supplementary Material

Refer to Web version on PubMed Central for supplementary material.

Acknowledgements

The authors thank Katerina Xenaki for important support at the beginning of this study, and Malgorzata Krawczyk-Durka for assistance. This study received funding from the European Research Council under the European Union's Horizon 2020 research and innovation programme (grant agreement No 677582). The European Research Council had no involvement in the study design, in the collection, analysis and interpretation of data, in the writing of the report and in the decision to submit the article for publication.

References

[1]. Moja L, Tagliabue L, Balduzzi S, Parmelli E, Pistotti V, Guarneri V, et al. Trastuzumab containing regimens for early breast cancer. Cochrane Database Syst Rev. 2012; (4)

[2]. Joerger M, Thurlimann B, Huober J. Small HER2-positive, node-negative breast cancer: who should receive systemic adjuvant treatment? Ann Oncol. 2011; 22:17–23. [PubMed: 20566473]

[3]. Cho HS, Mason K, Ramyar KX, Stanley AM, Gabelli SB, Denney DW Jr. et al. Structure of the extracellular region of HER2 alone and in complex with the Herceptin fab. Nature. 2003; 421:756–760. [PubMed: 12610629]

[4]. Slamon D, Eiermann W, Robert N, Pienkowski T, Martin M, Press M, et al. Adjuvant trastuzumab in HER2-positive breast cancer. N Engl J Med. 2011; 365:1273–1283. [PubMed: 21991949]

[5]. Cortazar P, Zhang L, Untch M, Mehta K, Costantino JP, Wolmark N, et al. Pathological complete response and long-term clinical benefit in breast cancer: the CTNeoBC pooled analysis. Lancet. 2014; 384:164–172. [PubMed: 24529560]

[6]. de Azambuja E, Holmes AP, Piccart-Gebhart M, Holmes E, Di Cosimo S, Swaby RF, et al. Lapatinib with trastuzumab for HER2-positive early breast cancer (NeoALTTO): survival outcomes of a randomised, open-label, multicentre, phase 3 trial and their association with pathological complete response. Lancet Oncol. 2014; 15:1137–1146. [PubMed: 25130998]

[7]. Gianni L, Eiermann W, Semiglazov V, Lluch A, Tjulandin S, Zambetti M, et al. Neoadjuvant and adjuvant trastuzumab in patients with HER2-positive locally advanced breast cancer (NOAH): follow-up of a randomised controlled superiority trial with a parallel HER2-negative cohort. Lancet Oncol. 2014; 15:640–647. [PubMed: 24657003]

[8]. Perez EA, Romond EH, Suman VJ, Jeong JH, Sledge G, Geyer CE Jr. et al. Trastuzumab plus adjuvant chemotherapy for human epidermal growth factor receptor 2-positive breast cancer: planned joint analysis of overall survival from NSABP B-31 and NCCTG N9831. J Clin Oncol. 2014; 32:3744–3752. [PubMed: 25332249]

[9]. Goldhirsch A, Gelber RD, Piccart-Gebhart MJ, de Azambuja E, Procter M, Suter TM, et al. 2 years versus 1 year of adjuvant trastuzumab for HER2-positive breast cancer (HERA): an open-label, randomised controlled trial. Lancet. 2013; 382:1021–1028. [PubMed: 23871490]

[10]. Hurvitz SA, Martin M, Symmans WF, Jung KH, Huang CS, Thompson AM, et al. Neoadjuvant trastuzumab, pertuzumab, and chemotherapy versus trastuzumab emtansine plus pertuzumab in patients with HER2-positive breast cancer (KRISTINE): a randomised, open-label, multicentre, phase 3 trial. Lancet Oncol. 2018; 19:115–126. [PubMed: 29175149]

[11]. Cobleigh MA, Vogel CL, Tripathy D, Robert NJ, Scholl S, Fehrenbacher L, et al. Multinational study of the efficacy and safety of humanized anti-HER2 monoclonal antibody in women who have HER2-overexpressing metastatic breast cancer that has progressed after chemotherapy for metastatic disease. J Clin Oncol. 1999; 17:2639–2648. [PubMed: 10561337]

[12]. Vogel CL, Cobleigh MA, Tripathy D, Gutheil JC, Harris LN, Fehrenbacher L, et al. Efficacy and safety of trastuzumab as a single agent in first-line treatment of HER2-overexpressing metastatic breast cancer. J Clin Oncol. 2002; 20:719–726. [PubMed: 11821453]

[13]. Krop IE, Kim SB, Martin AG, LoRusso PM, Ferrero JM, Badovinac-Crnjevic T, et al. Trastuzumab emtansine versus treatment of physician's choice in patients with previously treated HER2-positive metastatic breast cancer (TH3RESA): final overall survival results from a randomised open-label phase 3 trial. Lancet Oncol. 2017; 18:743–754. [PubMed: 28526538]

[14]. von Minckwitz G, Huang CS, Mano MS, Loibl S, Mamounas EP, Untch M, et al. Trastuzumab emtansine for residual invasive HER2-positive breast cancer. N Engl J Med. 2019; 380(7):617–628. [PubMed: 30516102]

[15]. Blackwell KL, Burstein HJ, Storniolo AM, Rugo H, Sledge G, Koehler M, et al. Randomized study of Lapatinib alone or in combination with trastuzumab in women with ErbB2-positive, trastuzumab-refractory metastatic breast cancer. J Clin Oncol. 2010; 28:1124–1130. [PubMed: 20124187]

[16]. von Minckwitz G, Procter M, de Azambuja E, Zardavas D, Benyunes M, Viale G, et al. Adjuvant pertuzumab and trastuzumab in early HER2-positive breast cancer. N Engl J Med. 2017; 377:122–131. [PubMed: 28581356]

[17]. Swain SM, Kim SB, Cortes J, Ro J, Semiglazov V, Campone M, et al. Pertuzumab, trastuzumab, and docetaxel for HER2-positive metastatic breast cancer (CLEOPATRA study): overall survival results from a randomised, doubleblind, placebo-controlled, phase 3 study. Lancet Oncol. 2013; 14:461–471. [PubMed: 23602601]

[18]. Banerjee SM, El-Sheikh S, Malhotra A, Mosse CA, Parker S, Williams NR, et al. Photodynamic therapy in primary breast cancer. J Clin Med. 2020; 9

[19]. van Straten D, Mashayekhi V, de Bruijn HS, Oliveira S, Robinson DJ. Oncologic photodynamic therapy: basic principles, current clinical status and future directions. Cancers (Basel). 2017:9.

[20]. Oleinick NL, Morris RL, Belichenko I. The role of apoptosis in response to photodynamic therapy: what, where, why, and how. Photochem Photobiol Sci. 2002; 1:1–21. [PubMed: 12659143]

[21]. Celli JP, Spring BQ, Rizvi I, Evans CL, Samkoe KS, Verma S, et al. Imaging and photodynamic therapy: mechanisms, monitoring, and optimization. Chem Rev. 2010; 110:2795–2838. [PubMed: 20353192]

[22]. Mitsunaga M, Ogawa M, Kosaka N, Rosenblum LT, Choyke PL, Kobayashi H. Cancer cell-selective in vivo near infrared photoimmunotherapy targeting specific membrane molecules. Nat Med. 2011; 17:1685–1691. [PubMed: 22057348]

[23]. Solban N, Rizvi I, Hasan T. Targeted photodynamic therapy. Lasers Surg Med. 2006; 38:522–531. [PubMed: 16671102]

[24]. Heukers R, van Bergen en Henegouwen PM, Oliveira S. Nanobody-photo-sensitizer conjugates for targeted photodynamic therapy. Nanomedicine. 2014; 10:1441–1451. [PubMed: 24394212]

[25]. van Driel P, Boonstra MC, Slooter MD, Heukers R, Stammes MA, Snoeks TJA, et al. EGFR targeted nanobody-photosensitizer conjugates for photodynamic therapy in a pre-clinical model of head and neck cancer. J Control Release. 2016; 229:93–105. [PubMed: 26988602]

[26]. Heukers R, Mashayekhi V, Ramirez-Escudero M, de Haard H, Verrips TC, van Bergen en Henegouwen PMP, et al. VHH-photosensitizer conjugates for targeted photodynamic therapy of met-overexpressing tumor cells. Antibodies. 2019; 8:26.

[27]. De Groof TWM, Mashayekhi V, Fan TS, Bergkamp ND, Sastre Torano J, van Senten JR, et al. Nanobody-targeted photodynamic therapy selectively kills viral GPCR-expressing glioblastoma cells. Mol Pharm. 2019; 16:3145–3156. [PubMed: 31244224]

[28]. de Bruijn HS, Mashayekhi V, Schreurs TJL, van Driel PBAA, Strijkers GJ, van Diest PJ, et al. Acute cellular and vascular responses to photodynamic therapy using EGFR-targeted nanobody-photosensitizer conjugates studied with intravital optical imaging and magnetic resonance imaging. Theranostics. 2020; 10(5):2436–2452. [PubMed: 32089747]

[29]. Hamers-Casterman C, Atarhouch T, Muyldermans S, Robinson G, Hamers C, Songa EB, et al. Naturally occurring antibodies devoid of light chains. Nature. 1993; 363:446–448. [PubMed: 8502296]

[30]. Kruwel T, Nevoltris D, Bode J, Dullin C, Baty D, Chames P, et al. In vivo detection of small tumour lesions by multi-pinhole SPECT applying a (99m)Tc-labelled nanobody targeting the epidermal growth factor receptor. Sci Rep. 2016; 6

[31]. van Brussel AS, Adams A, Oliveira S, Dorresteijn B, El Khattabi M, Vermeulen JF, et al. Hypoxia-targeting fluorescent nanobodies for optical molecular imaging of pre-invasive breast cancer. Mol Imaging Biol. 2016; 18:535–544. [PubMed: 26589824]

[32]. Vaidyanathan G, McDougald D, Choi J, Koumarianou E, Weitzel D, Osada T, et al. Preclinical evaluation of 18F-labeled anti-HER2 nanobody conjugates for imaging HER2 receptor expression by immuno-PET. J Nucl Med. 2016; 57:967–973. [PubMed: 26912425]

[33]. Keyaerts M, Xavier C, Heemskerk J, Devoogdt N, Everaert H, Ackaert C, et al. Phase I study of 68Ga-HER2-nanobody for PET/CT assessment of HER2 expression in breast carcinoma. J Nucl Med. 2016; 57:27–33. [PubMed: 26449837]

[34]. Lv G, Qiu L, Sun Y, Li K, Liu Q, Zhao Q, et al. PET imaging of tumor PD-L1 expression with a highly specific non-blocking nanobody. J Nucl Med. 2020; 61(1):117–122. [PubMed: 31253743]

[35]. Prantner AM, Yin C, Kamat K, Sharma K, Lowenthal AC, Madrid PB, et al. Molecular imaging of Mesothelin-expressing ovarian cancer with a human and mouse cross-reactive nanobody. Mol Pharm. 2018; 15:1403–1411. [PubMed: 29462558]

[36]. Chatalic KL, Veldhoven-Zweistra J, Bolkestein M, Hoeben S, Koning GA, Boerman OC, et al. A novel (1)(1)(1)in-labeled anti-prostate-specific membrane antigen Nanobody for targeted SPECT/CT imaging of prostate cancer. J Nucl Med. 2015; 56:1094–1099. [PubMed: 25977460]

[37]. van Driel PB, van der Vorst JR, Verbeek FP, Oliveira S, Snoeks TJ, Keereweer S, et al. Intraoperative fluorescence delineation of head and neck cancer with a fluorescent anti-epidermal growth factor receptor nanobody. Int J Cancer. 2014; 134:2663–2673. [PubMed: 24222574]

[38]. Debie P, Vanhoeij M, Poortmans N, Puttemans J, Gillis K, Devoogdt N, et al. Improved Debulking of peritoneal tumor implants by near-infrared fluorescent nanobody image guidance in an experimental mouse model. Mol Imaging Biol. 2018; 20:361–367. [PubMed: 29090412]

[39]. Dekempeneer Y, Back T, Aneheim E, Jensen H, Puttemans J, Xavier C, et al. Labeling of anti-HER2 nanobodies with astatine-211: optimization and the effect of different coupling reagents on their in vivo behavior. Mol Pharm. 2019; 16:3524–3533. [PubMed: 31268724]

[40]. Choi J, Vaidyanathan G, Koumarianou E, Kang CM, Zalutsky MR. Astatine-211 labeled anti-HER2 5F7 single domain antibody fragment conjugates: radiolabeling and preliminary evaluation. Nucl Med Biol. 2018; 56:10–20. [PubMed: 29031230]

[41]. Xavier C, Blykers A, Vaneycken I, D'Huyvetter M, Heemskerk J, Lahoutte T, et al. (18)F-nanobody for PET imaging of HER2 overexpressing tumors. Nucl Med Biol. 2016; 43:247–252. [PubMed: 27067045]

[42]. Pruszynski M, Koumarianou E, Vaidyanathan G, Revets H, Devoogdt N, Lahoutte T, et al. Improved tumor targeting of anti-HER2 nanobody through N-succinimidyl 4-guanidinomethyl-3-iodobenzoate radiolabeling. J Nucl Med. 2014; 55:650–656. [PubMed: 24578241]

[43]. Heukers R, Vermeulen JF, Fereidouni F, Bader AN, Voortman J, Roovers RC, et al. Endocytosis of EGFR requires its kinase activity and N-terminal transmembrane dimerization motif. J Cell Sci. 2013; 126:4900–4912. [PubMed: 23943881]

[44]. Oliveira S, van Dongen GA, Stigter-van Walsum M, Roovers RC, Stam JC, Mali W, et al. Rapid visualization of human tumor xenografts through optical imaging with a near-infrared fluorescent anti-epidermal growth factor receptor nanobody. Mol Imaging. 2012; 11:33–46. [PubMed: 22418026]

[45]. Kijanka M, Warnders FJ, El Khattabi M, Lub-de Hooge M, van Dam GM, Ntziachristos V, et al. Rapid optical imaging of human breast tumour xenografts using anti-HER2 VHHs site-directly conjugated to IRDye 800CW for image-guided surgery. Eur J Nucl Med Mol Imaging. 2013; 40:1718–1729. [PubMed: 23778558]

[46]. Oliveira S, Heukers R, Sornkom J, Kok RJ, van Bergen En Henegouwen PM. Targeting tumors with nanobodies for cancer imaging and therapy. J Control Release. 2013; 172:607–617. [PubMed: 24035975]

[47]. van Leeuwen-van Zaane F, Gamm UA, van Driel PB, Snoeks TJ, de Bruijn HS, van der Ploeg-van den Heuvel A, et al. In vivo quantification of the scattering properties of tissue using multi-diameter single fiber reflectance spectroscopy. Biomed Opt Express. 2013; 4:696–708. [PubMed: 23667786]

[48]. Hu Z, Rao B, Chen S, Duanmu J. Targeting tissue factor on tumour cells and angiogenic vascular endothelial cells by factor VII-targeted verteporfn photo-dynamic therapy for breast cancer in vitro and in vivo in mice. BMC Cancer. 2010; 10:235. [PubMed: 20504328]

[49]. Duanmu J, Cheng J, Xu J, Booth CJ, Hu Z. Effective treatment of chemoresistant breast cancer in vitro and in vivo by a factor VII-targeted photodynamic therapy. Br J Cancer. 2011; 104:1401–1409. [PubMed: 21427724]

[50]. Stuchinskaya T, Moreno M, Cook MJ, Edwards DR, Russell DA. Targeted photodynamic therapy of breast cancer cells using antibody-phthalocyanine-gold nanoparticle conjugates. Photochem Photobiol Sci. 2011; 10:822–831. [PubMed: 21455532]

[51]. Obaid G, Chambrier I, Cook MJ, Russell DA. Cancer targeting with biomole-cules: a comparative study of photodynamic therapy efficacy using antibody or lectin conjugated phthalocyanine-PEG gold nanoparticles. Photochem Photobiol Sci. 2015; 14:737–747. [PubMed: 25604735]

[52]. de Bruijn HSMV, Schreurs TJL, van Driel PBAA, Strijkers GJ, van Diest PJ, Lowik CWGM, Seynhaeve ALB, ten Hagen TLM, Prompers JJ, van Bergen en Henegouwen PMP, Robinson DJ, et al. Acute cellular and vascular responses to photodynamic therapy using EGFR-targeted nanobody-photosensitizer conjugates studied with intravital optical imaging and magnetic resonance imaging. Theranostics. 2019

[53]. Debie P, Van Quathem J, Hansen I, Bala G, Massa S, Devoogdt N, et al. Effect of dye and conjugation chemistry on the biodistribution profile of near-infrared-labeled nanobodies as tracers for image-guided surgery. Mol Pharm. 2017; 14:1145–1153. [PubMed: 28245129]

[54]. Beltran Hernandez I, Rompen R, Rossin R, Xenaki KT, Katrukha EA, Nicolay K, et al. Imaging of tumor spheroids, dual-isotope SPECT, and autoradiographic analysis to assess the tumor uptake and distribution of different nanobodies. Mol Imaging Biol. 2019; 21(6):1079–1088. [PubMed: 30859470]

[55]. Middelburg TA, Van Zaane F, De Bruijn HS, Van Der Ploeg-van den Heuvel A, Sterenborg HJ, Neumann HA, et al. Fractionated illumination at low fluence rate photodynamic therapy in mice. Photochem Photobiol. 2010; 86:1140–1146. [PubMed: 20553407]

[56]. Peng W, de Bruijn HS, Farrell E, Sioud M, Mashayekhi V, Oliveira S, et al. Epidermal growth factor receptor (EGFR) density may not be the only determinant for the efficacy of EGFR-targeted photoimmunotherapy in human head and neck cancer cell lines. Lasers Surg Med. 2018; 50:513–522. [PubMed: 29777587]

[57]. Korsak B, Almeida GM, Rocha S, Pereira C, Mendes N, Osorio H, et al. Porphyrin modified trastuzumab improves efficacy of HER2 targeted photodynamic therapy of gastric cancer. Int J Cancer. 2017; 141:1478–1489. [PubMed: 28639285]

[58]. Ito K, Mitsunaga M, Nishimura T, Saruta M, Iwamoto T, Kobayashi H, et al. Near-infrared photochemoimmunotherapy by photoactivatable bifunctional antibody-drug conjugates targeting human epidermal growth factor receptor 2 positive cancer. Bioconjug Chem. 2017; 28:1458–1469. [PubMed: 28402624]

[59]. Pye H, Butt MA, Funnell L, Reinert HW, Puccio I, Rehman Khan SU, et al. Using antibody directed phototherapy to target oesophageal adenocarcinoma with heterogeneous HER2 expression. Oncotarget. 2018; 9:22945–22959. [PubMed: 29796164]

[60]. Sato K, Choyke PL, Kobayashi H. Photoimmunotherapy of gastric cancer peritoneal carcinomatosis in a mouse model. PLoS One. 2014; 9:e113276. [PubMed: 25401794]

[61]. Ito K, Mitsunaga M, Nishimura T, Kobayashi H, Tajiri H. Combination photo-immunotherapy with monoclonal antibodies recognizing different epitopes of human epidermal growth factor receptor 2: an assessment of phototherapeutic effect based on fluorescence molecular imaging. Oncotarget. 2016; 7:14143–14152. [PubMed: 26909859]

[62]. Li B, Meng Y, Zheng L, Zhang X, Tong Q, Tan W, et al. Bispecific antibody to ErbB2 overcomes trastuzumab resistance through comprehensive blockade of ErbB2 heterodimerization. Cancer Res. 2013; 73:6471–6483. [PubMed: 24046294]

[63]. Allison RR, Downie GH, Cuenca R, Hu XH, Childs CJ, Sibata CH. Photosensitizers in clinical PDT. Photodiagn Photodyn Ther. 2004; 1:27–42.

[64]. Shams M, Owczarczak B, Manderscheid-Kern P, Bellnier DA, Gollnick SO. Development of photodynamic therapy regimens that control primary tumor growth and inhibit secondary disease. Cancer Immunol Immunother. 2015; 64:287–297. [PubMed: 25384911]

[65]. Zhang NZ, Bai S, Cai XJ, Li LB. Inhibitory and immunological effects induced by the combination of photodynamic therapy and dendritic cells on mouse transplanted hepatoma. Photodiagn Photodyn Ther. 2016; 13:201–204.

[66]. Kleinovink JW, van Driel PB, Snoeks TJ, Prokopi N, Fransen MF, Cruz LJ, et al. Combination of photodynamic therapy and specific immunotherapy efficiently eradicates established tumors. Clin Cancer Res. 2016; 22:1459–1468. [PubMed: 26546617]

[67]. Beltran Hernandez I, Yu Y, Ossendorp F, Korbelik M, Oliveira S. Preclinical and clinical evidence of immune responses triggered in oncologic photodynamic therapy: clinical recommendations. J Clin Med. 2020; 9

[68]. Kallioniemi OP, Kallioniemi A, Kurisu W, Thor A, Chen LC, Smith HS, et al. ERBB2 amplification in breast cancer analyzed by fluorescence in situ hybridization. Proc Natl Acad Sci U S A. 1992; 89:5321–5325. [PubMed: 1351679]

[69]. Gutierrez C, Schif R. HER2: biology, detection, and clinical implications. Arch Pathol Lab Med. 2011; 135:55–62. [PubMed: 21204711]

[70]. Cui S, Yin D, Chen Y, Di Y, Chen H, Ma Y, et al. In vivo targeted deep-tissue photodynamic therapy based on near-infrared light triggered upconversion nano-construct. ACS Nano. 2013; 7:676–688. [PubMed: 23252747]

[71]. Moore LS, de Boer E, Warram JM, Tucker MD, Carroll WR, Korb ML, et al. Photoimmunotherapy of residual disease after incomplete surgical resection in head and neck cancer models. Cancer Med. 2016; 5:1526–1534. [PubMed: 27167827]

[72]. Lutje S, Heskamp S, Franssen GM, Frielink C, Kip A, Hekman M, et al. Development and characterization of a theranostic multimodal anti-PSMA targeting agent for imaging, surgical guidance, and targeted photodynamic therapy of PSMA-expressing tumors. Theranostics. 2019; 9:2924–2938. [PubMed: 31244933]

[73]. Bossuyt V, Provenzano E, Symmans WF, Boughey JC, Coles C, Curigliano G, et al. Recommendations for standardized pathological characterization of residual disease for

neoadjuvant clinical trials of breast cancer by the BIG-NABCG collaboration. Ann Oncol. 2015; 26:1280–1291. [PubMed: 26019189]

[74]. Cain H, Macpherson IR, Beresford M, Pinder SE, Pong J, Dixon JM. Neoadjuvant therapy in early breast cancer: treatment considerations and common debates in practice. Clin Oncol (R Coll Radiol). 2017; 29:642–652. [PubMed: 28669449]

[75]. Voduc KD, Cheang MC, Tyldesley S, Gelmon K, Nielsen TO, Kennecke H. Breast cancer subtypes and the risk of local and regional relapse. J Clin Oncol. 2010; 28:1684–1691. [PubMed: 20194857]

[76]. Jia H, Jia W, Yang Y, Li S, Feng H, Liu J, et al. HER-2 positive breast cancer is associated with an increased risk of positive cavity margins after initial lumpectomy. World J Surg Oncol. 2014; 12:289. [PubMed: 25241216]

[77]. Kijanka M, Dorresteijn B, Oliveira S, van Bergen en Henegouwen PM. Nanobody-based cancer therapy of solid tumors. Nanomedicine (London). 2015; 10:161–174.

[78]. D'Huyvetter M, Vincke C, Xavier C, Aerts A, Impens N, Baatout S, et al. Targeted radionuclide therapy with A 177Lu-labeled anti-HER2 nanobody. Theranostics. 2014; 4:708–720. [PubMed: 24883121]

[79]. Chanier T, Chames P. Nanobody engineering: toward next generation immunotherapies and immunoimaging of cancer. Antibodies (Basel). 2019:8.

[80]. Gray MA, Tao RN, DePorter SM, Spiegel DA, McNaughton BR. A nanobody activation immunotherapeutic that selectively destroys HER2-positive breast cancer cells. Chembiochem. 2016; 17:155–158. [PubMed: 26556305]

[81]. Lin L, Li L, Zhou C, Li J, Liu J, Shu R, et al. A HER2 bispecific antibody can be efficiently expressed in Escherichia coli with potent cytotoxicity. Oncol Lett. 2018; 16:1259–1266. [PubMed: 29963199]

[82]. Iqbal N, Iqbal N. Human epidermal growth factor receptor 2 (HER2) in cancers: overexpression and therapeutic implications. Mol Biol Int. 2014; 2014:852748. [PubMed: 25276427]

[83]. Yan M, Schwaederle M, Arguello D, Millis SZ, Gatalica Z, Kurzrock R. HER2 expression status in diverse cancers: review of results from 37,992 patients. Cancer Metastasis Rev. 2015; 34:157–164. [PubMed: 25712293]

Europe PMC Funders Author Manuscripts

Europe PMC Funders Author Manuscripts

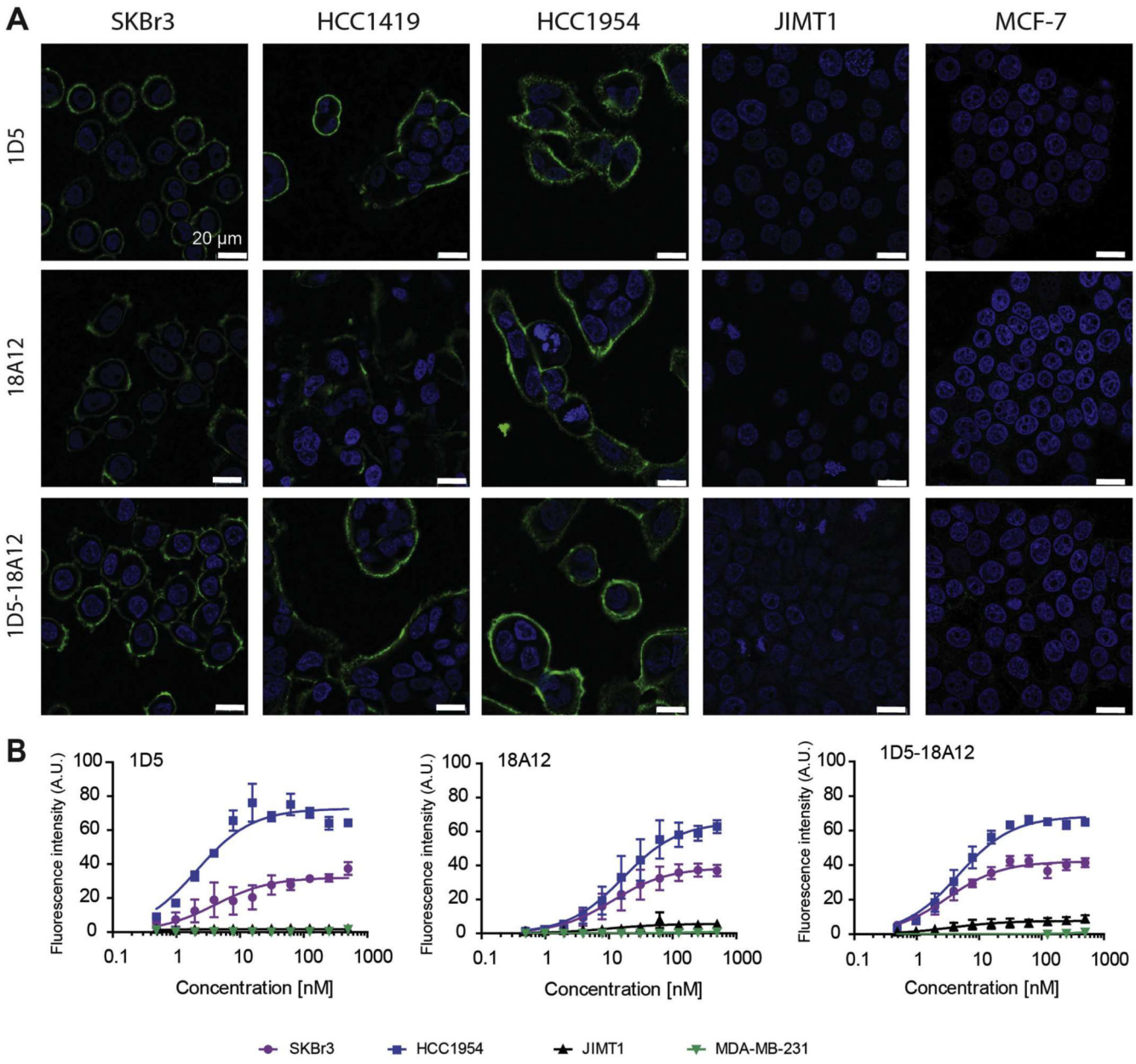

Fig. 1.

The selected nanobodies are HER2 specific. A. The HER2 overexpressing cell lines; SKBr3, HCC1419 and HCC1954, and the low HER2 expressing cell line JIMT1 and MCF-7, were incubated with the nanobodies, monovalent (1D5 and 18A12) or bivalent (1D5-18A12), at 50 nM concentration, and imaged using confocal microscopy (same imaging settings for each cell line, scale bar = 20 µm). B. All selected nanobodies bind to cell lines according to their HER2 expression level: HCC1954 > SKBr3 > JIMT1 and not to MDA-MB-231 cells. Detection of bound nanobodies was performed through primary and secondary antibodies, fluorescence intensity at 800 nm.

Europe PMC Funders Author Manuscripts

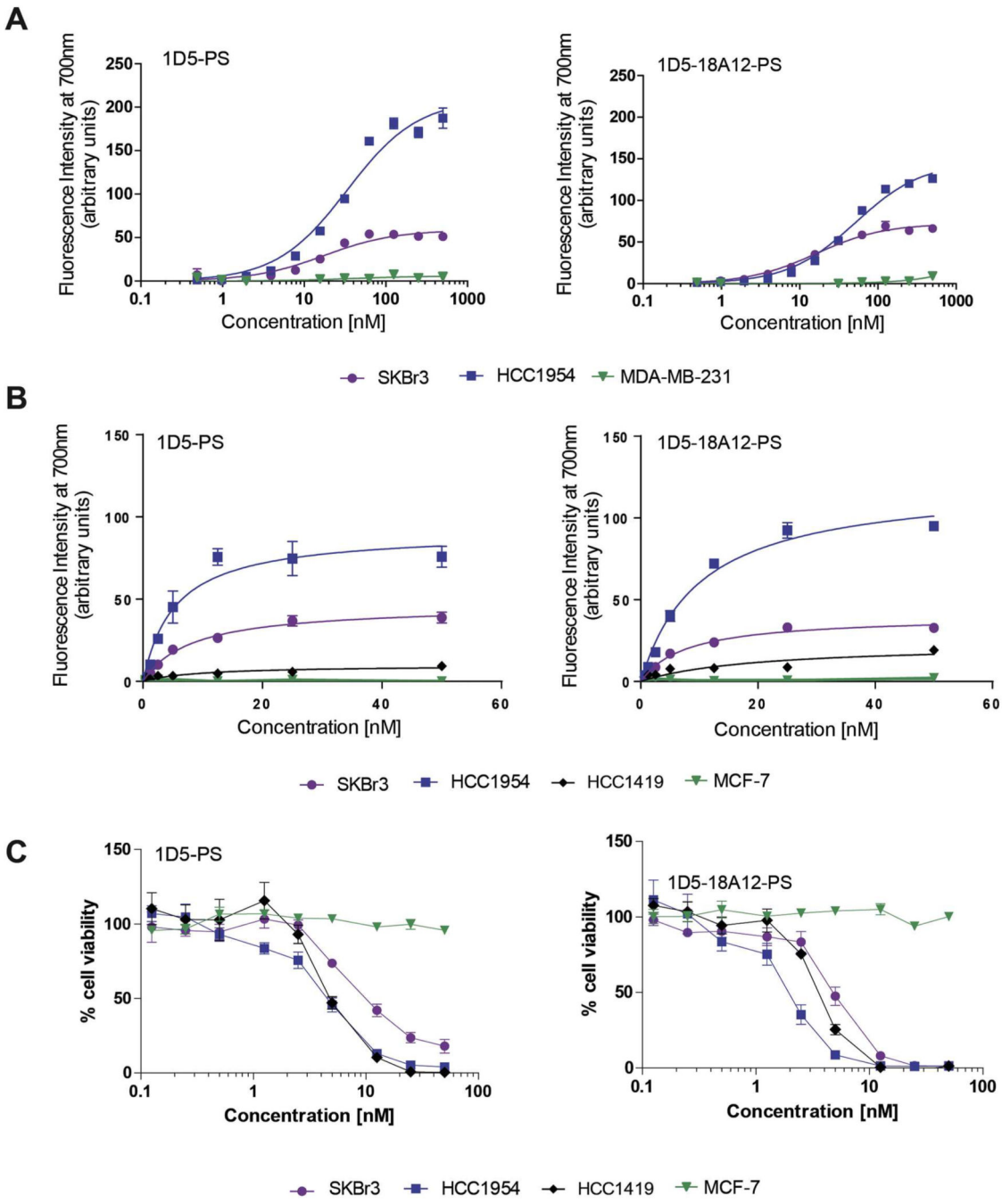

Fig. 2.

Nanobody-PS conjugates bind to cell lines according to their HER2 expression levels and upon illumination induce cytotoxicity to cells with high HER2 expression. A. Dilution series of 1D5-PS and 1D5-18A12-PS were incubated with cells for 1 h 30 min at 4 °C to determine apparent affinity. Bound nanobodies are directly detected through fluorescence of the PS. B. Total fluorescence intensity associated with cells after 30 min incubation at 37 °C with a concentration range of 1D5-PS or 1D5-18A12-PS. C. Cell viability determined 24 h after

illumination with 10 J·cm^{-2}. PDT with HER2 overexpressing cells and low HER2 expressing cells and 1D5-PS or 1D5-18A12-PS.

Europe PMC Funders Author Manuscripts

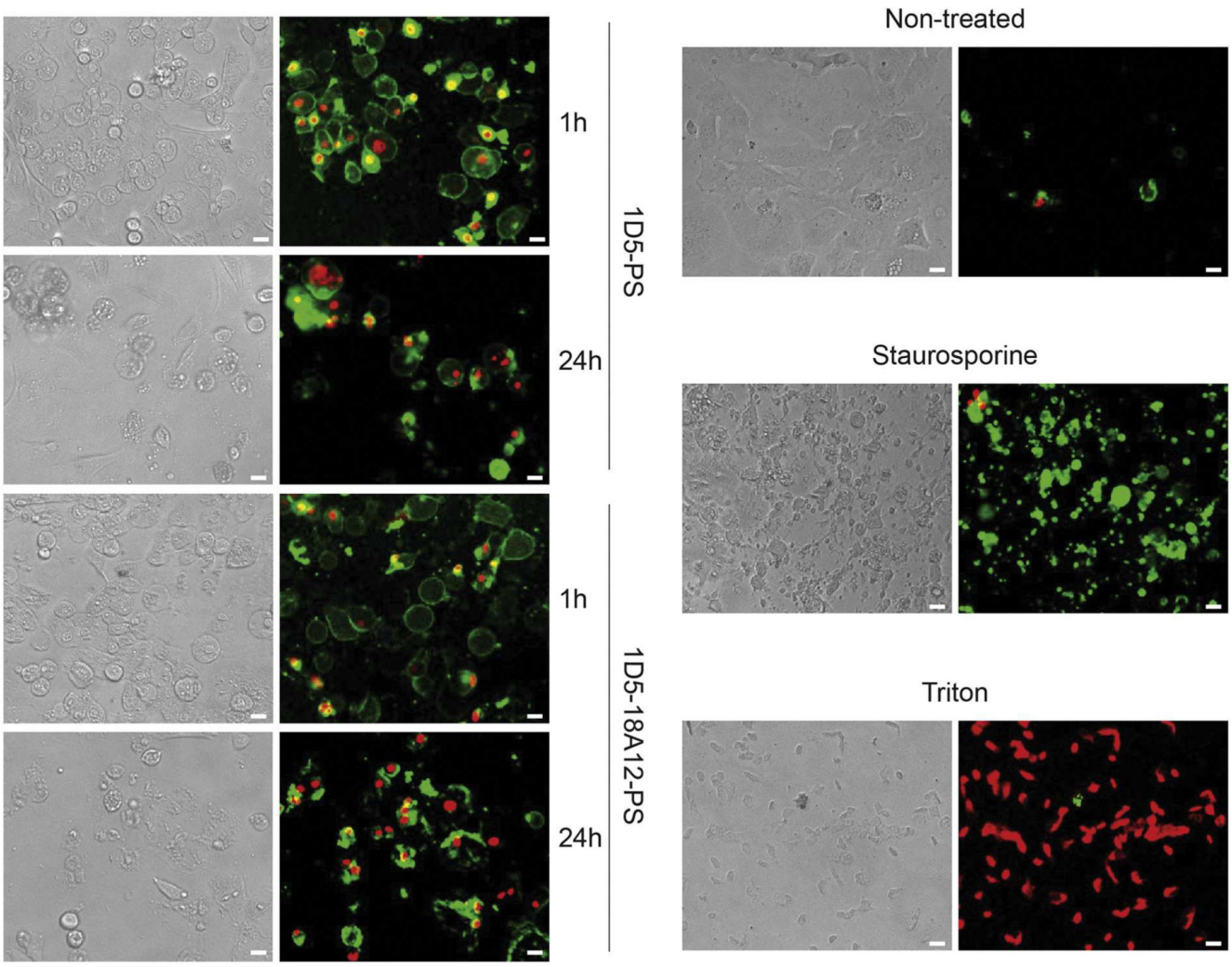

Fig. 3.

Nanobody-targeted PDT induces changes in morphology and cell death. HER2-positive HCC1954 were incubated with 25 nM nanobody-PS, 1D5-PS (upper left row) and 1D5-18A12 (lower left row), followed by light illumination (10 J/cm^2 of light dose). Apoptotic cells were detected with Annexin V-FITC (green), whereas necrotic cells with propidium iodide (red) staining 1 h and 24 h after light illumination. The increase of propidium iodide staining shows the toxic effect of PDT increased between 1 h and 24 h. As a control for apoptotic and necrotic cell death, non-treated HCC1954 cells were incubated with Staurosporine or Triton respectively (right row). Pictures were obtained with an EVOS Microscope equipped with 10× objective. Scale = 20 μm. (For interpretation of the references to colour in this figure legend, the reader is referred to the web version of this article.)

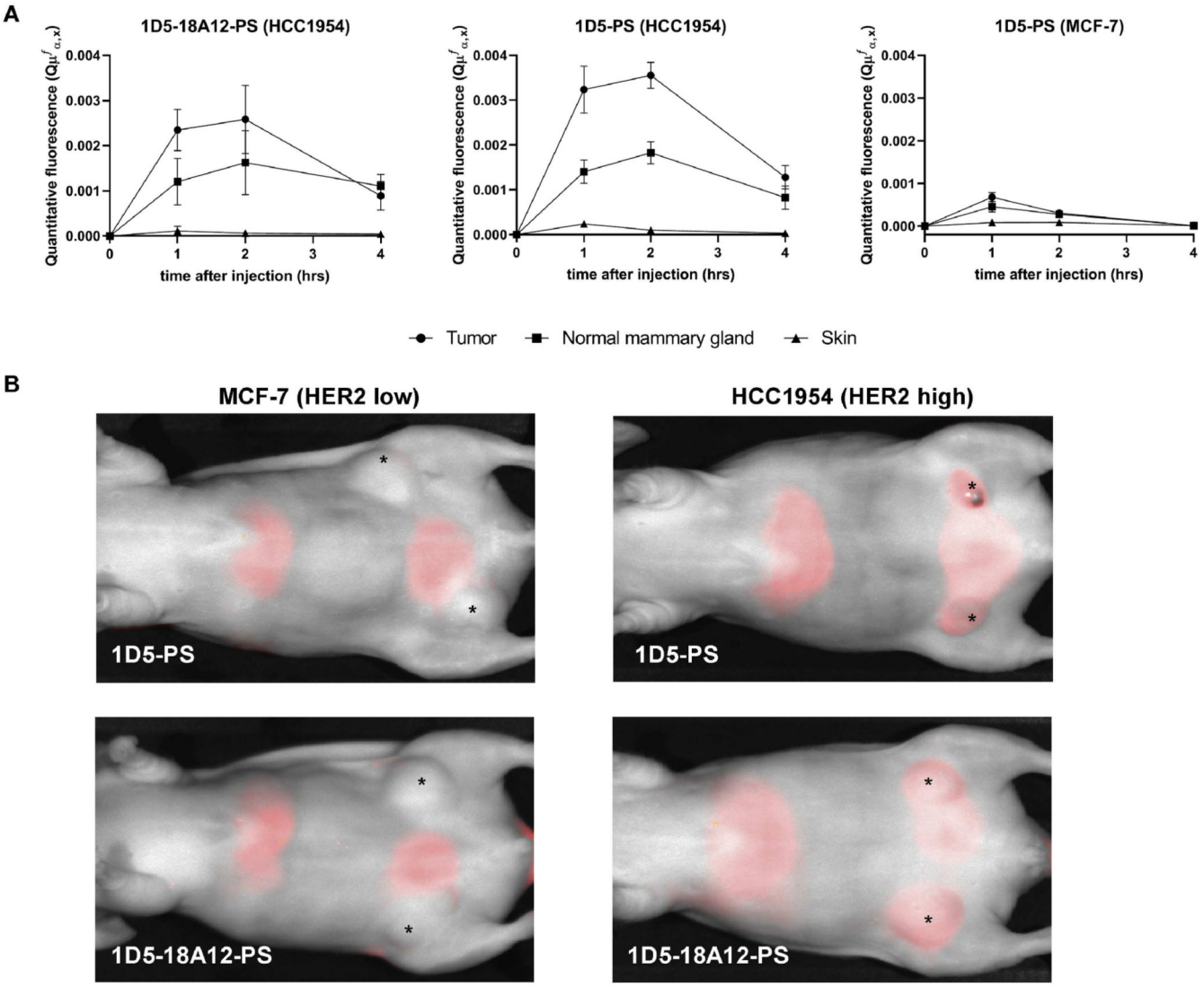

Fig. 4.

Quantitative fluoresence spectroscopy and fluorescence images after intravenous injection of nanobody-PS. A. The quantitative fluorescence of 1D5-PS and 1D5-18A12-PS at 2 h post injection was significantly higher in HCC1954 tumors than of 1D5-PS in MCF-7 tumors (respectively $p < .001$ and $p < .05$). The maximum amount of 1D5-PS and 1D5-18A12-PS was observed at 2 h post injection. B. Fluorescence images (at 700 nm) of mice bearing MCF-7 (A + B) or HCC1954 (C + D) tumors, 1 h 45 after intravenous injection of 1D5-PS or 1D5-18A12-PS, showing accumulation of both nanobody-PS in tumors with high HER2 expression. In contrast, in the low HER2 expressing tumors none or less accumulation of both nanobody-PS is shown. Beside tumor uptake, uptake of the nanobody-PS was also seen in the bladder, as the clearance of the nanobody-PS is through the kidneys, and liver. *Orthotopic breast tumor *in situ*.

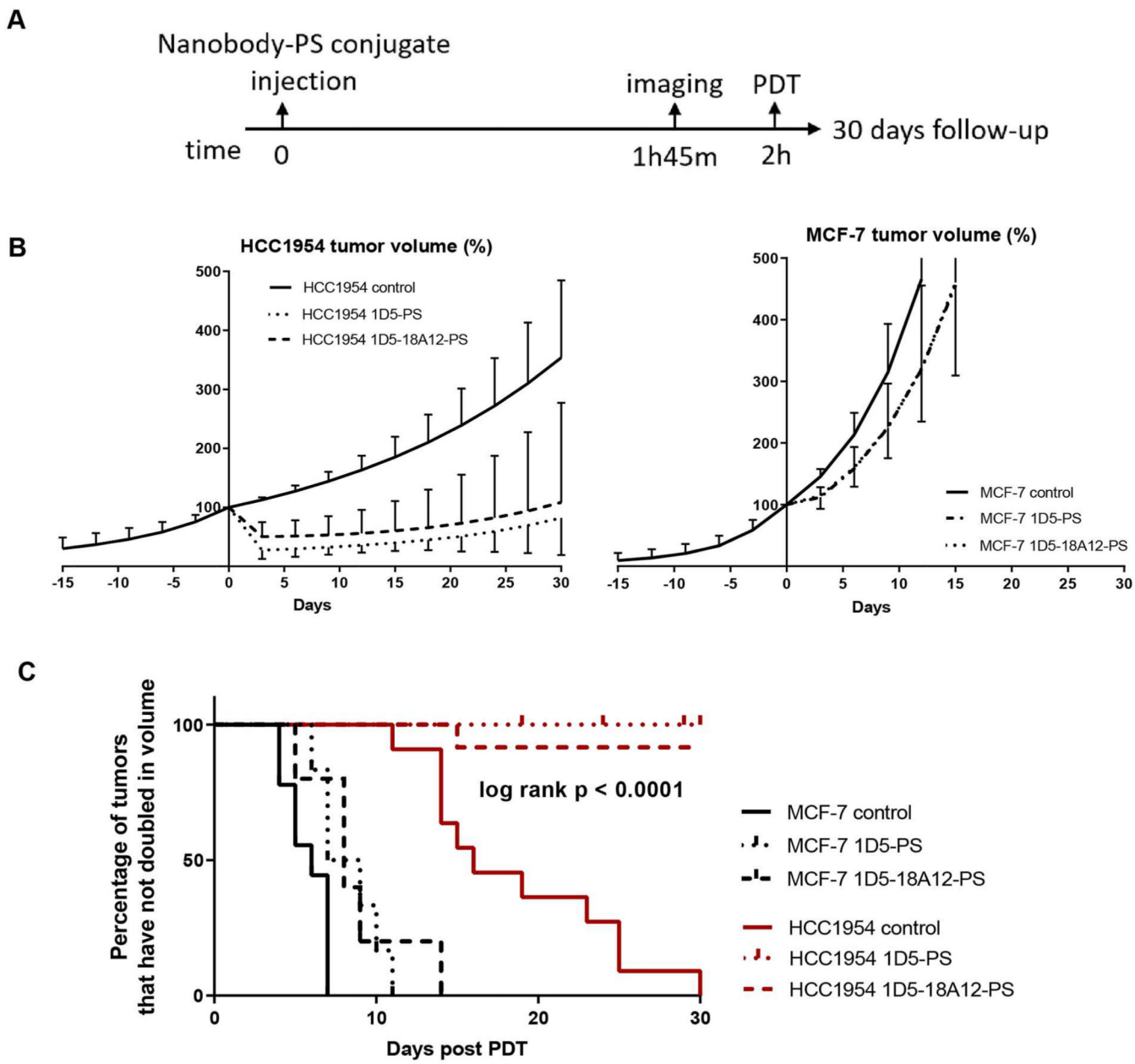

Fig. 5.

Nanobody-PS photodynamic therapy induced tumor regression in high HER2 expressing breast tumors. A. Experimental protocol of photodynamic therapy in vivo. Injection of nanobody-PS conjugates was performed at time 0, imaging with Pearl Imaging System at 1 h 45 and illumination was performed 2 h after injection. B. Mice injected with 1D5-PS (n = 8 HCC1954, n = 7 MCF-7) or 1D5-18A12-PS (n = 13 HCC1954, n = 6 MCF-7), or vehicle as control (n = 11 HCC1954, n = 9 MCF-7), were subsequently illuminated and tumor growth monitored, here depicted in percentage. Day 0 as day of illumination. C. Kaplan Meier curve of the percentage of tumors that have not double in volume (200%) after 30 days.